Applied Physics Letters

Proximity-induced anisotropic magnetoresistance in magnetized topological insulators

Cite as: Appl. Phys. Lett. **118**, 232402 (2021); https://doi.org/10.1063/5.0052301
Submitted: 30 March 2021 . Accepted: 20 May 2021 . Published Online: 11 June 2021

Joseph Sklenar, Yingjie Zhang, Matthias Benjamin Jungfleisch, Youngseok Kim, Yiran Xiao, Gregory J. MacDougall, Matthew J. Gilbert, Axel Hoffmann, Peter Schiffer, and Nadya Mason

Applied Physics Letters ARTICLE scitation.org/journal/apl

Proximity-induced anisotropic magnetoresistance in magnetized topological insulators

Cite as: Appl. Phys. Lett. **118**, 232402 (2021); doi: 10.1063/5.0052301
Submitted: 30 March 2021 · Accepted: 20 May 2021 ·
Published Online: 11 June 2021

Joseph Sklenar,[1,2,a)] Yingjie Zhang,[3] Matthias Benjamin Jungfleisch,[4,5] Youngseok Kim,[6] Yiran Xiao,[1] Gregory J. MacDougall,[1] Matthew J. Gilbert,[6,7] Axel Hoffmann,[1,3,4,6] Peter Schiffer,[1,8,9] and Nadya Mason[1]

AFFILIATIONS

[1]Department of Physics Materials Research Laboratory, University of Illinois, Urbana, Illinois 61801, USA
[2]Department of Physics and Astronomy, Wayne State University, Detroit, Michigan 48202, USA
[3]Department of Materials Science and Engineering, University of Illinois, Urbana, Illinois 61801, USA
[4]Materials Science Division, Argonne National Laboratory, Lemont, Illinois 60439, USA
[5]Department of Physics and Astronomy, University of Delaware, Newark, Delaware 19716, USA
[6]Department of Electrical and Computer Engineering, University of Illinois, Urbana, Illinois 61801, USA
[7]Department of Electrical Engineering, Stanford University, Stanford, California 94305, USA
[8]Department of Physics, Yale University, New Haven, Connecticut 06520, USA
[9]Department of Applied Physics, Yale University, New Haven, Connecticut 06520, USA

[a)]Author to whom correspondence should be addressed: jnsklenar@wayne.edu

ABSTRACT

Topological insulators (TIs) host spin-momentum locked surface states that are inherently susceptible to magnetic proximity modulations, making them promising for nano-electronic, spintronic, and quantum computing applications. While much effort has been devoted to studying (quantum) anomalous Hall effects in magnetic magnetically doped TIs, the inherent magnetoresistance (MR) properties in magnetic proximity-coupled surface states remain largely unexplored. Here, we directly exfoliate Bi_2Se_3 TI flakes onto a magnetic insulator, yttrium iron garnet, and measure the MR at various temperatures. We experimentally observe an anisotropic magnetoresistance that is consistent with a magnetized surface state. Our results indicate that the TI has magnetic anisotropy out of the sample plane, which opens an energy gap between the surface states. By applying a magnetic field along any in-plane orientation, the magnetization of the TI rotates toward the plane and the gap closes. Consequently, we observe a large (~6.5%) MR signal that is attributed to an interplay between coherent rotation of magnetization within a topological insulator and abrupt switching of magnetization in the underlying magnetic insulator.

In metallic ferromagnetic films, anisotropic magnetoresistance (AMR)[1] refers to the dependence of a film's resistivity on the orientation of magnetization with respect to the current passing through it. In spintronic research, AMR plays a central role in a wide variety of experimental contexts. For example, the AMR of a ferromagnetic layer can be used to detect magnetization dynamics[2–4] within magnetic heterostructures designed so that spin torques drive the magnetization. Often, TIs are involved in these experiments because they are capable of generating large spin torques[5–7] and easily facilitate spin-to-charge conversion.[8,9] On the other hand, the use of TIs as a source of AMR in these spintronic experiments is, relative to torque effects, underexplored. Because of the strong spin–orbit coupling intrinsic to TIs, it is anticipated that AMR effects in TIs should be large.[10]

We report a magnetoresistance effect that is phenomenologically consistent with a proximity-AMR predicted to exist in undoped, magnetic surface states of a TI that are adjacent to a ferromagnetic insulator.[10] In this report, we will refer to this effect as a proximty-AMR, owing to the fact that the dependence of this AMR on magnetization orientation differs from conventional AMR behavior. The proximity-AMR of the TI does not arise from magnetic impurities; instead, this AMR originates from an energy gap opening at the conducting surface states. Similar effects are expected in antiferromagnetic Dirac semimetals, where the Néel vector orientation determines high and low resistance states.[11] The proximty-AMR we measure has a high resistance when magnetization is perpendicular to the surface and a low resistance when magnetization lies in the plane of the surface. In

comparison, conventional AMR of metallic ferromagnets has a high resistance when the magnetization is parallel to the current and a low resistance when perpendicular to the current.[1] The maximum percent change we find in resistance due to proximity-AMR is roughly 6.5% at 1.8 K. This is significantly larger than spin Hall magnetoresistance (0.01%), an AMR-like effect induced in metals with strong spin–orbit coupling by magnetic insulators.[12]

In order to study the proximity-AMR effect of the TI, we use bilayers consisting of a TI on a ferromagnetic insulator, which provides an exchange interaction at the interface to "proximity"-magnetize the TI surface state.[13–16] We note that the other strategy to magnetize a TI is to intentionally dope the material with magnetic elements.[17] That approach has been key to the observation of the quantum anomalous Hall effect within a magnetic TI.[18,19] More recently, in the magnetically doped TI, AMR behavior has been observed[20] and used to characterize an asymmetric magnetoresistance effect due to magnon scattering. To rule out additional AMR effects that can arise from magnetic impurities, we chose to employ the magnetic proximity effect so that the AMR is intrinsic to the surface-state.[10]

We mechanically exfoliated Bi_2Se_3 flakes[21–24] directly onto the magnetic insulator yttrium iron garnet (YIG), as illustrated and shown through atomic force microscopy in Figs. 1(a) and 1(b). The YIG is 25 nm thick and grown on a gadolinium gallium garnet (GGG) substrate via sputtering,[25–27] and the flake is 30 nm thick. The YIG behaves as an in-plane ferromagnet with a low coercive field (< 2 Oe) from 1.8 to 300 K.[25–27] Magnetometry over the relevant experimental temperature range is shown in Fig. 1(c). Exfoliation of the Bi_2Se_3 leads to variable flake sizes, thicknesses (ranging from 25 to 60 nm), and resistivities. The most resistive flakes in this thickness range show proximity-induced ferromagnetic magnetotransport effects, as described in this manuscript. More conductive flakes often show no proximity-induced ferromagnetic behavior; instead, these flakes reproduce previously reported weak anti-localization effects observed in TIs.[28–30]

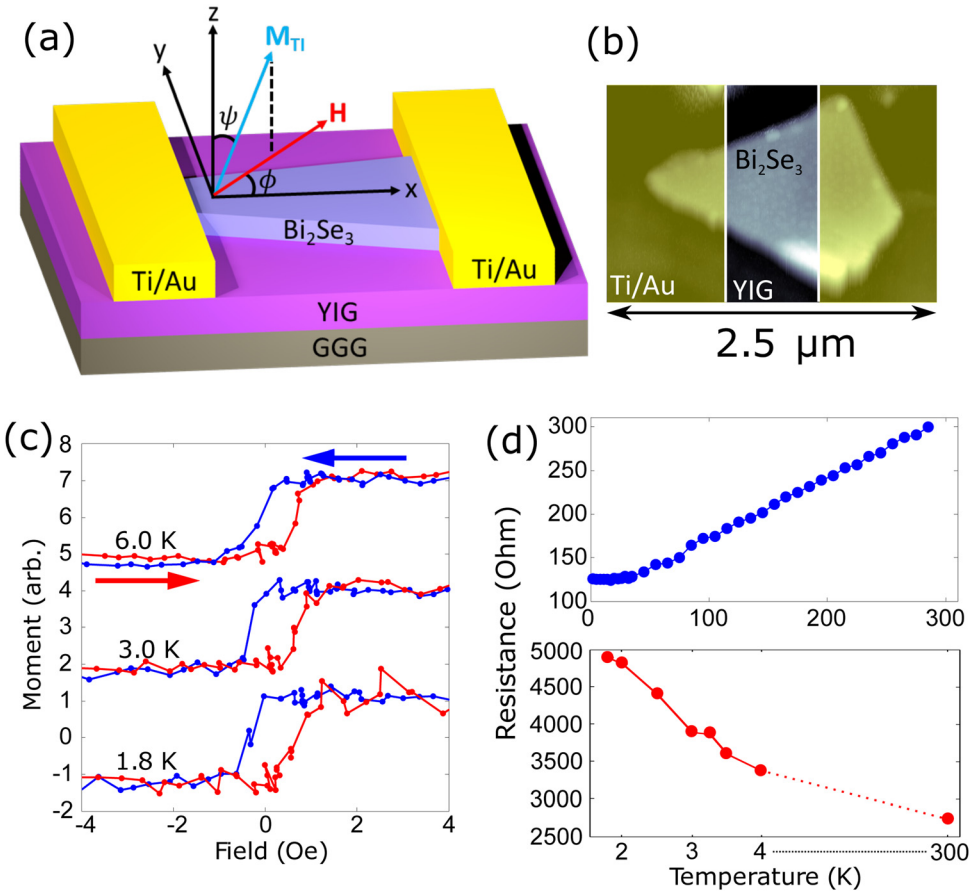

FIG. 1. (a) An illustration of a 30 nm Bi_2Se_3 flake exfoliated on YIG and contacted by Ti/Au electrodes. The coordinate system depicts that the current flows in the *x*-direction and an external magnetic field is applied in the *xy* plane at an angle ϕ. The magnetization of the TI cants toward the in-plane direction of the external field as described by the polar angle ψ. (b) Atomic force microscopy image of a TI flake. False shaded yellow rectangles represent the patterned Ti/Au electrodes. (c) SQUID magnetometry of the bare YIG film shown over the temperature range where we observed ferromagnetic effects in the magnetoresistance. Note that the coercive field of the YIG is less than 2 Oe over the relevant temperature range. (d) Resistance vs temperature for a resistive Bi_2Se_3 flake (red) compared with a conductive flake (blue) that are exfoliated on the same YIG substrate.

The measurement coordinate system and relevant field and magnetization vectors are illustrated in Fig. 1(a). The magnetic field, H, is applied at an in-plane angle ϕ relative to the current. Because of perpendicular magnetic anisotropy (PMA) in the TI,[31] the magnetization of the TI (M_{TI}) is not generally co-linear to the applied field. A polar angle, ψ, is used to describe the orientation of M_{TI}. We make two-point measurements of the resistance across flakes as a function of applied magnetic field. In Fig. 1(d), we plot the temperature-dependent resistance of the flake shown in Fig. 1(b), as well as that of a similarly sized more conductive flake. The more resistive flake (red) displays a significant rise in resistance as the temperature is lowered, while the more conductive flake (blue) shows a decrease in resistance. These are characteristic behaviors of TIs with Fermi level within the bulk gap (semiconducting behavior) and within the bulk conduction band (metallic behavior).[32] Magnetoresistance of the conductive flake is shown in the supplementary material Fig. S8, and no ferromagnetic behavior is observed. We note that due to the insulating nature of the substrate, electrostatic charging effects were problematic. The most robust samples were those measured in a two-point configuration, i.e., electrodes patterned transverse to the current often failed. Thus, we do not have Hall resistivity data as a companion to our longitudinal data.

Below 4 K, the magnetoresistance of the resistive Bi_2Se_3/YIG bilayers exhibits a strong 6.5% change in the MR as a function of field. In this low-temperature range, there are also pronounced ferromagnetic hysteresis effects in the MR signal. In Fig. 2(a), we plot the MR curves for different temperatures at $\phi = 90°$. Here, current and field are perpendicular to one another and the field is swept from negative to positive values. At 4 K, there are negative dips in the magnetoresistance that are hysteretic; a similar effect has been previously observed and attributed to enhanced conduction from domain walls in the adjacent magnetic insulator[13] (see supplementary material Section 1.2). Below 4 K, a pronounced magnetoresistance peak emerges, which causes the zero-field resistance to considerably increase. In Figs. 2(b) and 2(c), we show the magnetoresistance at 1.8 K for data taken at both $\phi = 0°$ and $\phi = 90°$. Unlike conventional AMR, we see a large signal when the field is applied in-plane-parallel and perpendicular to the current. Furthermore, when we apply a field of 5 kOe and measure the MR as the field is rotated in the xy plane, we observe no change in the resistance as a function of ϕ; this is markedly different behavior from conventional AMR in metallic ferromagnets (see supplementary material Section 3). A near equal amplitude and ferromagnetic signal at both $\phi = 0°$ and $\phi = 90°$, combined with no variation in the resistance as a function of ϕ at large fields, is consistent with the TI having PMA where a high resistance state occurs at remanence from the magnetization pointing out-of-plane. By applying an in-plane magnetic field at any orientation, we rotate the magnetization from a high resistance state to a low resistance state. We note that there is some weak anisotropy in the shape of the AMR signal when comparing $\phi = 0°$ and $\phi = 90°$. In supplementary material Section 4, we discuss possible origins of this anisotropy. We now describe theoretical modeling and

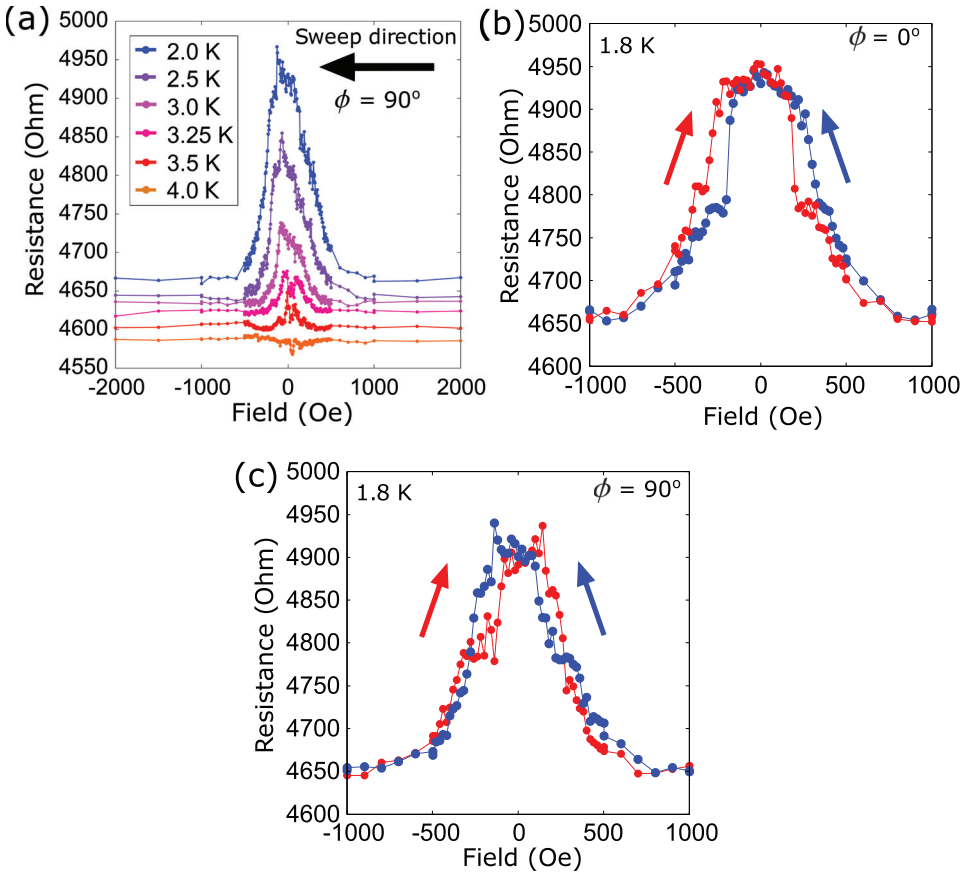

FIG. 2. (a) The temperature-dependent magnetoresistance for an in-plane applied field at $\phi = 90°$ is shown. The field is swept from positive to negative, and a resistance offset is manually added for visibility purposes. A magnetoresistance peak emerges below 4.0 K, which saturates at fields above a few hundred Oe. (b) and (c) We show experimental data at 1.8 K for $\phi = 0°$ and $\phi = 90°$, respectively. Magnetic hysteresis is clearly observed for both configurations, and the presence of a magnetoresistance peak at both orientations is inconsistent with the conventional AMR of metallic ferromagnets.

micromagnetic simulations, which support the assertion of PMA in the magnetized TI layer.

We attribute the low-temperature MR peak to AMR in the TI arising from proximity-induced, perpendicular magnetization. Theoretically, if the Fermi energy of a TI is close to the Dirac point, a magnetized TI should have PMA.[31] In fact, neutron scattering measurements have provided evidence for magnetization with PMA induced in Bi_2Se_3 by the magnetic insulator, EuS, which has in-plane anisotropy.[15] In Fig. 3(a), we illustrate how proximity-AMR arises in a TI with PMA. At zero-field, the magnetization of the TI is nearly parallel to the z-direction (out-of-plane) opening a gap in the surface states; canting from the z-direction is expected if the underlying magnetic insulator has in-plane anisotropy. When the magnetization has a large out-of-plane component, the resistance is then expected to be (relatively) large. As a field is applied in the plane of the sample, the magnetization rotates toward the plane and the gap will close. Throughout this process, the resistance continuously decreases as the out-of-plane component of the magnetization is reduced. We emphasize that the angular dependence of the AMR in the TI only relies on the polar angle, $\psi(H)$, which describe the orientation of the out-of-plane magnetization as a function of the applied field. This is in contrast with conventional AMR,[1] spin Hall magnetoresistance,[12] and AMR induced by Rashba spin–orbit coupling,[33] where, quite generally, the magnetoresistance depends on the orientation of the magnetization relative to the current.

To theoretically model the data, we need to obtain the field evolution of $\psi(H)$. Previously, a diffusive transport model was formulated to explain how the resistance of a TI changes as the surface state becomes gapped by the magnetization.[10] With $\psi(H)$, this transport model can be utilized, and the angular-dependence of proximity-AMR can be written as[10]

$$\rho_{xx} = \frac{\hbar h}{e^2 E_F \tau_e} \frac{1+\xi^2\cos\psi^2}{1-\xi^2\cos\psi^2}, \tag{1}$$

$$\xi = \frac{\zeta}{\sqrt{1+\zeta^2\cos\psi^2}}. \tag{2}$$

In the above expression $\zeta = \Delta/E_F$, Δ is the proximity-induced exchange energy, while E_F is the Fermi energy relative to the Dirac point when there is no magnetization in the z-direction. Additionally, τ_e is the electronic elastic scattering rate, e is the charge of the electron, h is Planck's constant, and $\hbar$ is the reduced Planck's constant.

A simple way to obtain $\psi(H)$ is to minimize a free energy expression that treats the TI as a magnetic thin film with perpendicular anisotropy,[34]

$$F = -HM_{TI}\sin\psi + 2\pi M_{TI}^2\cos^2\psi - K_u\cos^2\psi, \tag{3}$$

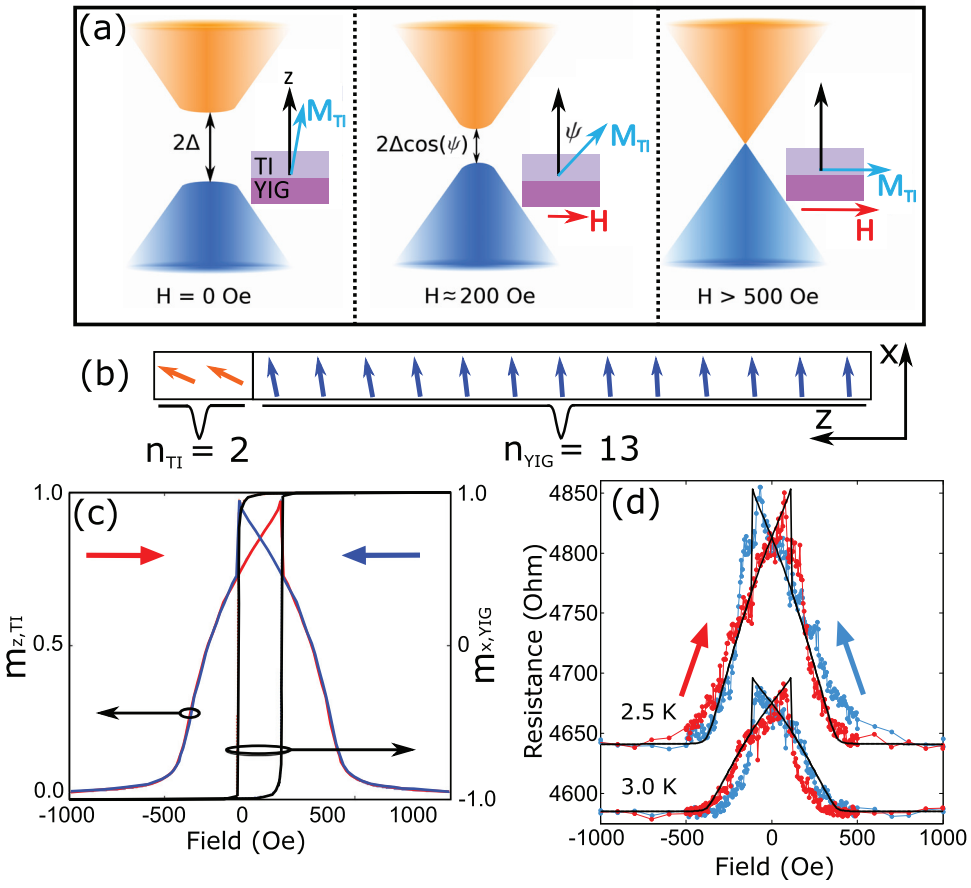

FIG. 3. (a) Illustration of the AMR mechanism in a proximity magnetized TI. Perpendicular magnetization induced in the TI by the YIG will open a gap (2Δ) between the surface states. Applying an in-plane field (H) rotates the magnetization (M_{TI}) toward the in-plane direction, which leads to a decrease in the bandgap. (b) We plot the remnant magnetic moment configuration of our micromagnetic simulations after a field is applied along the +x-direction. Note how there is appreciable spin canting out-of-plane near the YIG-TI interface due to exchange coupling between competing anisotropies. (c) We plot the field evolution of the z-component of the TI magnetization and the x-component of the YIG magnetization obtained from micromagnetic simulations. The red and blue arrows indicate the sweep direction of the external field. The z-component of the magnetization in the TI is greatest right at the switching field of the YIG (offset from zero), which leads to a kink in the magnetoresistance. The circled pairs of curves and the corresponding black arrows indicate which curves correspond to the x(z)-component of the magnetization. (d) We fit the magnetoresistance, informed by micromagnetic simulations, to the resistance expression in Eq. (1). Red and blue arrows indicate sweep direction.

where K_u is a uniaxial anisotropy coefficient. With $\psi(H)$ acquired, the resistance line shape can, in principle, be fit with just two parameters, Δ/E_F and K_u. However, this approach does not capture the hysteretic features in the line shape; it only describes the smoothly varying component of the resistance. This is not surprising, given that this treatment of the data is phenomenologically similar to that observed with conventional AMR behavior when an applied field is along a hard axis.[35] Still, the free energy model has utility as a simple approach to estimate Δ/E_F and K_u, and we employ this model to do so. In Fig. 4(a), we plot Δ/E_F as a function of temperature as extracted from our free energy analysis for $\phi = 90°$. We find that Δ/E_F increases in a linear manner between 3.5 and 2.0 K from approximately 5% to 14%. From the same analysis, we can estimate K_u and we find that, within experimental error, it was independent of temperature corresponding to an effective uniaxial field of nearly 14 kOe. A more detailed discussion of this analysis is found in supplementary material Section 4. We note that similar results are obtained by performing the same analysis for $\phi = 0°$.

A more faithful representation of the magnetic bilayer system can be constructed using micromagnetic simulations, where a ferromagnet with in-plane anisotropy (the YIG) is exchange coupled to an out-of-plane ferromagnet (the TI surface). Using Object Oriented MicroMagnetic framework (OOMMF),[36] we built a 1D discretized lattice of 13 layers (YIG) with in-plane anisotropy coupled with 2 layers (TI) having perpendicular anisotropy. An illustration of a micromagnetic remnant moment configuration is shown in Fig. 3(b). Material parameters were informed by our data as well as the literature, and a detailed discussion of simulations is found in supplementary material Section 5. We simulated the application of an external field and recorded the magnetization as a function of field. At every field step in the simulation, we averaged and normalized the magnetization to a unit vector. The z-component of the magnetization unit vector, as a function of external field, is $\psi(H)$; used in conjunction with Eq. (1), the magnetoresistance is modeled.

In Fig. 3(c), we plot micromagnetic simulations of the averaged x- and z-components of the magnetization in the YIG and the TI, respectively. In Fig. 3(d), we plot magnetoresistance generated from micromagnetic simulations as black lines on top of the experimental data. Taken together, these simulations reveal that the large, smoothly varying component of the signal originates from the tendency of the TI-magnetization to *coherently rotate* as an in-plane field is applied. However, because the YIG has in-plane anisotropy, the YIG-magnetization will *suddenly switch* as the field is reversed. Because the two materials have orthogonal anisotropies, exchange coupling causes the remanent magnetization state of TI to be slightly canted toward the sample plane. When the magnetic field is reversed, the magnetization of the TI begins to rotate further out of the sample plane causing the resistance to further increase and leading to a "spike" in the resistance offset from remanence. The resistance is largest just before the switching field of the YIG, after which the magnetization of the TI further rotates toward the plane lowering the resistance.

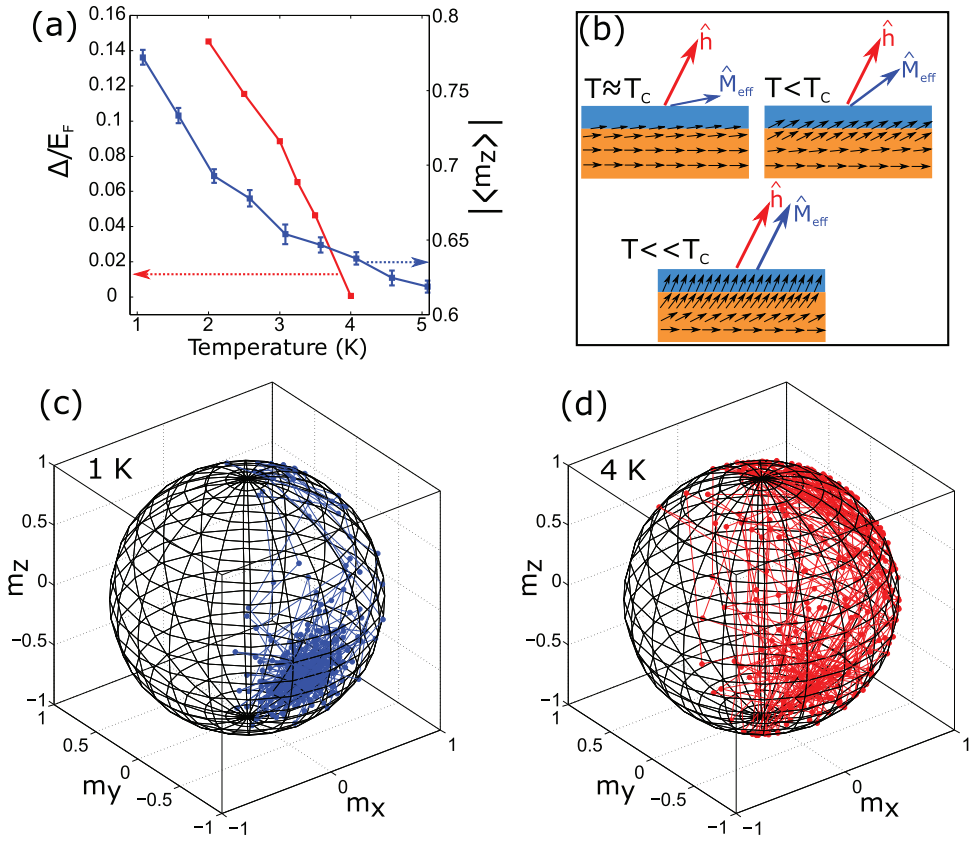

FIG. 4. (a) Δ/E_F is plotted as a function of temperature as red squares for $\phi = 90°$. The micromagnetically obtained, temporally and spatially averaged, z-component of the magnetization in the TI is plotted as a function of temperature as blue squares. (b) An illustration of the magnetic ordering within the TI. From left to right, the diagrams indicate the effective field that the TI (drawn in blue) experiences along with a potential magnetization configuration. The magnetization in the TI tends to order along an axis canted from the out-of-plane axis due to competing anisotropies between YIG and the TI, and this direction is indicated as $\hat{h}$. The averaged, effective magnetization of the TI is illustrated by the quantity $\hat{M}_{eff}$.(c) and (d) We plot the time trajectories of the spatially averaged magnetization of the TI as a unit vector on the unit sphere at 1 K and 4 K, based on micromagnetic simulations.

Our experimental data are phenomenologically consistent with theory, which only takes into account surface-state contributions to the AMR. However, we need to consider whether bulk conduction in the TI could also contribute to AMR-like behaviors.[12] Recent studies have shown that even for cases where there is significant bulk conduction, the magnetotransport is sensitive to the surface states.[37,38] Further, in a metal or TI adjacent to a ferromagnet, proximity effects are usually observed to extend less than 3 nm into the non-magnetic metal.[15,39] This implies that ferromagnetic proximity effects, observed in a TI adjacent to a magnet, only exist at and near the surface of a TI. We also note some indirect evidence, which suggests that, for the resistive samples we measure, the Fermi level lies within the bulk bandgap. Hall measurements of our bulk $BiSe_3$ single crystal (which is grown with excess Se[40]) reveal a carrier density[40] of 5×10^{17} cm^{-3}, a value consistent with carrier densities measured in ARPES studies, which observe the Fermi energy within or near the bulk bandgap.[41] This is consistent with the observed increase in sample resistance as the temperature is lowered in our resistive samples.

We posit that the temperature dependence of Δ/E_F arises from the magnetic ordering of the TI near 4 K, as illustrated in Fig. 4(b). Alternatively, a change in magnetic anisotropy as a function of temperature[31] could describe the temperature dependence, but this effect is extremely small over the temperature range we measure (see supplementary material Section 6). To investigate thermal fluctuations over the temperature range, we experimentally measured and performed temperature-dependent micromagnetic simulations. We precondition the micromagnetic calculations using material parameters obtained from modeling the line shape of the experimental data. In Fig. 4(a), we plot the time and spatially averaged z-component of the magnetization in the TI as blue squares. From 1 K to 5 K, the out-of-plane magnetic moment decreases monotonically due to thermal fluctuations. In Figs. 4(c) and 4(d), we plot the time-dependent trajectories of the spatially averaged TI magnetization on a unit sphere at 1 K and 4 K at zero-field. At 1 K, the magnetization tends to be aligned with PMA ($\hat{z}$), slightly canted toward the YIG magnetization ($\hat{x}$). At 4 K, the magnetization frequently switches between the two canted static equilibrium directions. All of these data taken together indicate that a low-temperature magnetic ordering effect is responsible for the emergence of proximity-AMR below 4 K.

In conclusion, we have reported an anisotropic magnetoresistance effect, which arises from a proximity-magnetized surface state of the TI. The change in the resistance is controlled by the component of the net magnetization, which is normal to the sample surface. This perpendicular magnetization opens a gap in the TI surface state, which leads to an increase in resistance. The resistance of the TI changes by 6.5%, which is significantly larger than similar effects induced by magnetic insulators into spin Hall metals.[12] By electrically gating the TI, one can tune the Fermi energy closer to the Dirac point and enhance this effect.

See the supplementary material section that houses additional magnetotransport data and analysis. Furthermore, simulation details are provided and other mechanisms for the temperature dependence observed in the data are discussed and ruled out.

AUTHORS' CONTRIBUTIONS

J.S and Y. Z. contributed equally to this work.

Work at The University of Illinois at Urbana-Champaign was supported by the National Science Foundation MRSEC program under NSF Award No. DMR-1720633. NM acknowledges support from the Army under No. W911NF-20–1-0024. G.J.M and Y.X. acknowledge support from the U.S. Department of Energy under Grant No. DE-SC0012368. Y.Z. acknowledges support from the University of Illinois. Work at Argonne, including YIG thin film growth, was supported by the U.S. Department of Energy, Office of Science, Materials Science and Engineering Division. All authors contributed to the data analysis and manuscript preparation.

DATA AVAILABILITY

The data that support the findings of this study are available from the corresponding author upon reasonable request.

REFERENCES

[1]T. McGuire and R. Potter, IEEE Trans. Magn. **11**, 1018 (1975).
[2]L. Liu, T. Moriyama, D. Ralph, and R. Buhrman, Phys. Rev. Lett. **106**, 036601 (2011).
[3]S. Langenfeld, V. Tshitoyan, Z. Fang, A. Wells, T. Moore, and A. Ferguson, Appl. Phys. Lett. **108**, 192402 (2016).
[4]J. Sklenar, W. Zhang, M. B. Jungfleisch, H. Saglam, S. Grudichak, W. Jiang, J. E. Pearson, J. B. Ketterson, and A. Hoffmann, Phys. Rev. B **95**, 224431 (2017).
[5]A. Mellnik, J. Lee, A. Richardella *et al.*, Nature **511**, 449 (2014).
[6]Y. Fan, P. Upadhyaya, X. Kou *et al.*, Nat. Mater. **13**, 699 (2014).
[7]J. Han, A. Richardella, S. A. Siddiqui, J. Finley, N. Samarth, and L. Liu, Phys. Rev. Lett. **119**, 077702 (2017).
[8]H. Wang, J. Kally, J. S. Lee, T. Liu, H. Chang, D. R. Hickey, K. A. Mkhoyan, M. Wu, A. Richardella, and N. Samarth, Phys. Rev. Lett. **117**, 076601 (2016).
[9]J.-C. Rojas-Sánchez, S. Oyarzún, Y. Fu, A. Marty *et al.*, Phys. Rev. Lett. **116**, 096602 (2016).
[10]T. Chiba, S. Takahashi, and G. E. Bauer, Phys. Rev. B **95**, 094428 (2017).
[11]L. Šmejkal, J. Železný, J. Sinova, and T. Jungwirth, Phys. Rev. Lett. **118**, 106402 (2017).
[12]H. Nakayama, M. Althammer, Y.-T. Chen *et al.*, Phys. Rev. Lett. **110**, 206601 (2013).
[13]P. Wei, F. Katmis, B. A. Assaf, H. Steinberg, P. Jarillo-Herrero, D. Heiman, and J. S. Moodera, Phys. Rev. Lett. **110**, 186807 (2013).
[14]M. Lang, M. Montazeri, M. C. Onbasli *et al.*, Nano Lett. **14**, 3459 (2014).
[15]F. Katmis, V. Lauter, F. S. Nogueira *et al.*, Nature **533**, 513 (2016).
[16]Y. Fanchiang, K. Chen, C. Tseng, C. Chen, C. Cheng, S. Yang, C. Wu, S. Lee, M. Hong, and J. Kwo, Nat. Commun. **9**, 223 (2018).
[17]Y. Chen, J.-H. Chu, J. Analytis *et al.*, Science **329**, 659 (2010).
[18]R. Yu, W. Zhang, H.-J. Zhang, S.-C. Zhang, X. Dai, and Z. Fang, Science **329**, 61 (2010).
[19]C.-Z. Chang, J. Zhang, X. Feng *et al.*, Science **340**, 1232003 (2013).
[20]K. Yasuda, A. Tsukazaki, R. Yoshimi, K. Takahashi, M. Kawasaki, and Y. Tokura, Phys. Rev. Lett. **117**, 127202 (2016).
[21]S. Cho, N. P. Butch, J. Paglione, and M. S. Fuhrer, Nano Lett. **11**, 1925 (2011).
[22]J. G. Checkelsky, Y. S. Hor, R. J. Cava, and N. Ong, Phys. Rev. Lett. **106**, 196801 (2011).
[23]D. Kim, S. Cho, N. P. Butch, P. Syers, K. Kirshenbaum, S. Adam, J. Paglione, and M. S. Fuhrer, Nat. Phys. **8**, 459 (2012).
[24]S. Cho, B. Dellabetta, A. Yang, J. Schneeloch, Z. Xu, T. Valla, G. Gu, M. J. Gilbert, and N. Mason, Nat. Commun. **4**, 1689 (2013).
[25]H. Chang, P. Li, W. Zhang, T. Liu, A. Hoffmann, L. Deng, and M. Wu, IEEE Magn. Lett. **5**, 1 (2014).
[26]S. Li, W. Zhang, J. Ding, J. E. Pearson, V. Novosad, and A. Hoffmann, Nanoscale **8**, 388 (2016).
[27]M. B. Jungfleisch, J. Ding, W. Zhang, W. Jiang, J. E. Pearson, V. Novosad, and A. Hoffmann, Nano Lett. **17**, 8 (2017).
[28]J. Chen, H. Qin, F. Yang *et al.*, Phys. Rev. Lett. **105**, 176602 (2010).
[29]M. Liu, J. Zhang, C.-Z. Chang *et al.*, Phys. Rev. Lett. **108**, 036805 (2012).
[30]Q. I. Yang, M. Dolev, L. Zhang *et al.*, Phys. Rev. B **88**, 081407 (2013).

[31]Y. G. Semenov, X. Duan, and K. W. Kim, Phys. Rev. B **86**, 161406 (2012).
[32]D. Kong, Y. Chen, J. J. Cha *et al.*, Nat. Nanotechnol. **6**, 705 (2011).
[33]H. Nakayama, Y. Kanno, H. An, T. Tashiro, S. Haku, A. Nomura, and K. Ando, Phys. Rev. Lett. **117**, 116602 (2016).
[34]S. Lee, S. Grudichak, J. Sklenar, C. Tsai, M. Jang, Q. Yang, H. Zhang, and J. B. Ketterson, J. Appl. Phys. **120**, 033905 (2016).
[35]T. G. Rijks, S. Lenczowski, R. Coehoorn, and W. De Jonge, Phys. Rev. B **56**, 362 (1997).
[36]M. J. Donahue and D. G. Porter, "OOMMF User's Guide, Version 1.0," Technical Report No. NISTIR 6376 (National Institute of Standards and Technology, Gaithersburg, MD, 1999).
[37]P. He, S. S.-L. Zhang, D. Zhu, Y. Liu, Y. Wang, J. Yu, G. Vignale, and H. Yang, Nat. Phys. **14**, 495 (2018).
[38]E. de Vries, S. Pezzini, M. Meijer, N. Koirala, M. Salehi, J. Moon, S. Oh, S. Wiedmann, and T. Banerjee, Phys. Rev. B **96**, 045433 (2017).
[39]C. Klewe, T. Kuschel, J.-M. Schmalhorst, F. Bertram, O. Kuschel, J. Wollschläger, J. Strempfer, M. Meinert, and G. Reiss, Phys. Rev. B **93**, 214440 (2016).
[40]A. Q. Chen, M. J. Park, S. T. Gill, Y. Xiao, D. Reig, I. Plessis, G. J. MacDougall, M. J. Gilbert, and N. Mason, Nat. Commun. **9**, 3478 (2018).
[41]J. G. Analytis, J.-H. Chu, Y. Chen, F. Corredor, R. D. McDonald, Z. Shen, and I. R. Fisher, Phys. Rev. B **81**, 205407 (2010).